Electronic Supplementary Information

A mononuclear nonheme {FeNO}^{6} complex: Synthesis and structural and spectroscopic characterization

Seungwoo Hong,[ab] James J. Yan,[c] Deepika G. Karmalkar,[a] Kyle D. Sutherlin,[c] Jin Kim,[a]
Yong-Min Lee,[a] Yire Goo,[a] Pradip K. Mascharak,*[d] Britt Hedman,*[e] Keith O. Hodgson,*[ce]
Kenneth D. Karlin,*[f] Edward I. Solomon,*[ce] and Wonwoo Nam*[a]

[a] *Department of Chemistry and Nano Science, Ewha Womans University, Seoul 03760, Korea*

[b] *Department of Chemistry, Sookmyung Women's University, Seoul 04310, Korea*

[c] *Department of Chemistry, Stanford University, Stanford, California 94305, USA*

[d] *Department of Chemistry and Biochemistry, University of California, Santa Cruz, California 95064, United States*

[e] *Stanford Synchrotron Radiation Lightsource, SLAC National Accelerator Laboratory, Stanford University, California 94025, USA*

[f] *Department of Chemistry, The Johns Hopkins University, Baltimore, Maryland 21218, United States*

* To whom correspondence should be addressed.
E-mail: edward.solomon@stanford.edu, bhedman@stanford.edu, hodgsonk@stanford.edu,
karlin@jhu.edu, wwnam@ewha.ac.kr

Table of Contents

Table S1 Crystallographic data and refinements for **1** and **2**

	1	2
Empirical formula	$C_{47}H_{52}FeN_5O_6P$	$C_{51}H_{94}FeN_7O_6$
Formula weight	869.75	957.18
Temperature (K)	120(2)	100(2)
Wavelength (Å)	0.71073	0.71073
Crystal system/space group	triclinic, P_1	monoclinic, $P_{21/c}$
Unit cell dimensions		
a (Å)	12.7848(8)	18.404(4)
b (Å)	13.0223(8)	18.521(4)
c (Å)	13.1304(9)	17.725(3)
α (°)	93.792(3)	90
β (°)	92.468(3)	102.745(3)
γ (°)	90.347(3)	90
Volume (Å^3)	2179.2(2)	5892.9(19)
Z	2	4
Calculated density (g/cm^{-3})	1.326	1.079
Absorption coefficient (mm^{-1})	0.467	0.303
Reflections collected	72796	10345
Independent reflections	10889	7108
Goodness-of-fit on F^2	1.027	1.063
R [$F^2 > 2\text{sigma}(F^2)$]	0.0348	0.0819
wR^2	0.0874	0.2515

Table S2 Selected bond distances (Å) and angles (°) for **1** and **2**

	1	**2**
Bond Distances (Å)		
Fe1-N1	1.8981(12)	1.899(3)
Fe1-N2	1.9013(12)	1.903(3)
Fe1-N3	1.8717(12)	1.889(4)
Fe1-N4	1.8664(12)	1.885(3)
Fe1-N5	1.6131(13)	-
Fe1-O1	-	2.068(4)
N5-O1		1.169(6)
N5-O2	-	1.269(7)
Bond Angles (°)		
N1-Fe1-N5	103.87(6)	-
N2-Fe1-N5	105.17(6)	-
N3-Fe1-N5	104.31(6)	-
N4-Fe1-N5	103.94(6)	-
N1-Fe1-O1	-	104.10(14)
N2-Fe1-O1	-	104.42(15)
N3-Fe1-O1	-	103.13(15)
N4-Fe1-O1	-	103.28(15)
Fe1-N5-O1	172.05(14)	-
Fe1-O1-N5	-	122.4(4)
O1-N5-O2	-	116.1(5)

Table S3 Experimental and calculated Mössbauer parameters (mm s^{-1}) of **1** and [(PaPy$_3$)Fe(NO)]$^{2+}$

	1	BP86 **1**	[(PaPy$_3$)Fe(NO)]$^{2+}$	BP86 [(PaPy$_3$)Fe(NO)]$^{2+}$
δ (mm s^{-1})	–0.19	–0.23	–0.05	–0.01
ΔE_Q (mm s^{-1})	3.29	3.28	0.85	0.402

Table S4 Comparison of crystal structure of **1** with crystal structures of known 5C ([Fe(TPP)NO](BF$_4$) and [Fe(OEP)(NO)](ClO$_4$) and 6C ([(PaPy$_3$)Fe^{III}(NO)]$^{2+}$ and [(^{NHC}L)Fe(NO)(ONO)](OTf)$_2$) {FeNO}^{6} compounds.

	1	[Fe(TPP)(NO)](BF$_4$)[a]	[Fe(OEP)NO](ClO$_4$)[b]	[(PaPy$_3$)Fe^{III}(NO)]$^{2+}$ [c]	[(^{NHC}L)FeNO(NO$_2$)](OTf)$_2$[d]
Fe-NO bond length (Å)	1.62	1.64/1.665	1.644	1.68	1.625
N-O bond length (Å)	1.17	1.153/1.124	1.112	1.14	1.162
Fe-N-O bond angle (°)	172.6	178.3/177.4	176.9	173.1	176.6
Average Fe-N$_{eq}$ bond length (Å)	1.89	1.986/1.990	1.994	1.98	2.008

[a]reference 13f in the main text. [b]W. R. Scheidt, Y. J. Lee, K. Hatano, *J. Am.Chem. Soc.*, 1984, **106**, 3191. [c]reference 14 in the main text. [d] reference 19 in the main text.

Table S5 EXAFS Least Square Fitting Results of **1**

component	coordination/path	$R(Å)^a$	$\sigma^2(Å^2)^b$	ΔE_0 (eV)	F^c
1	1 Fe-NO	1.62	291		
2	4 Fe-N	1.89	276		
3	2 N-O MS	3.03	120		
4	8 Fe-C	2.93	695	–2.0	0.26
5	16 C-N MS	3.13	695		
6	8 C-O MS	4.11	851		
7	8 C-C MS	4.67	686		

[a]The estimated standard deviations for the distances are in the order of ± 0.02 Å. [b]The σ^2 values are multiplied by 10^5. [c]Error is given by $\Sigma[(\chi_{obsd} - \chi_{calcd})^2 k^6]/\Sigma[(\chi_{obsd})^2 k^6]$. The S_0^2 factor was set at 1.

Table S6 Comparison of pre-edge intensity between **1** and $[(PaPy_3)Fe(NO)]^{2+}$

Pre-Edge (in energy)	**1**	$[(PaPy_3)Fe(NO)]^{2+}$
7112.1 eV	16	-
7113.0 eV	-	9
7113.3 eV	11	-
Total	27(0.3)	9(0.6)

Table S7 Comparison of experimental and computational geometric parameters for **1** and $[(PaPy_3)Fe^{III}(NO)]^{2+}$ using the BP86 functional

	Crystal **1**	EXAFS **1**	BP86 **1**	Crystal $[(PaPy_3)Fe^{III}(NO)]^{2+}$	BP86 $[(PaPy_3)Fe^{III}(NO)]^{2+}$
Fe-NO bond length (Å)	1.62	1.62	1.60	1.68	1.67
N-O bond length (Å)	1.17	-	1.18	1.14	1.16
Fe-N-O bond angle (°)	172.6	-	175.4	173.1	171.4
Average Fe-N_{eq} bond length (Å)	1.89	1.89	1.90	1.98	2.01
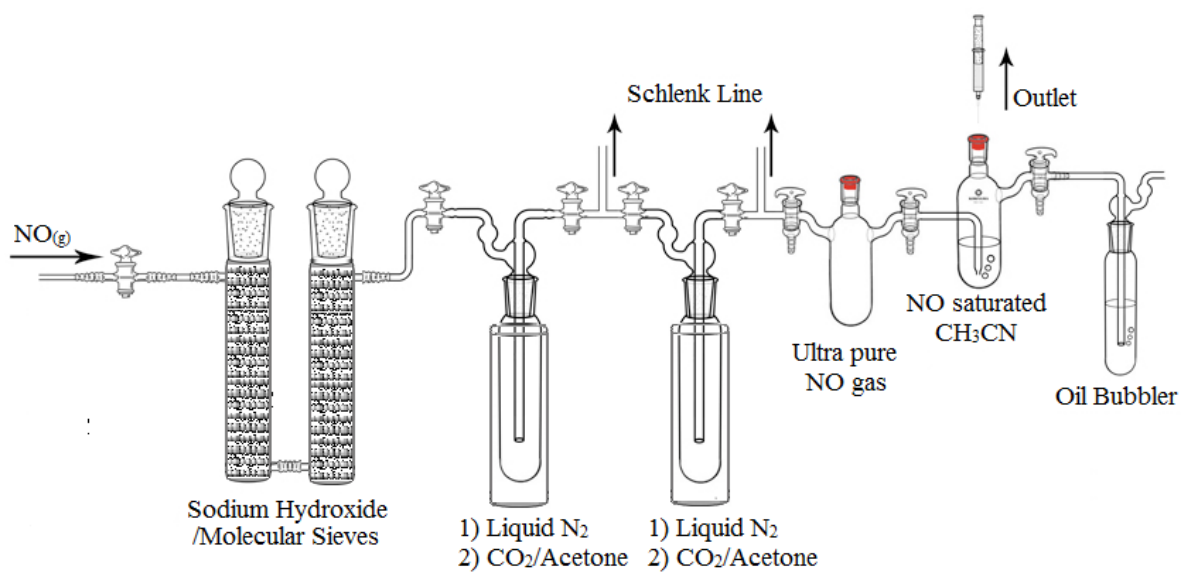
Fig. S1 Schematic diagram showing the purification setup for NO.
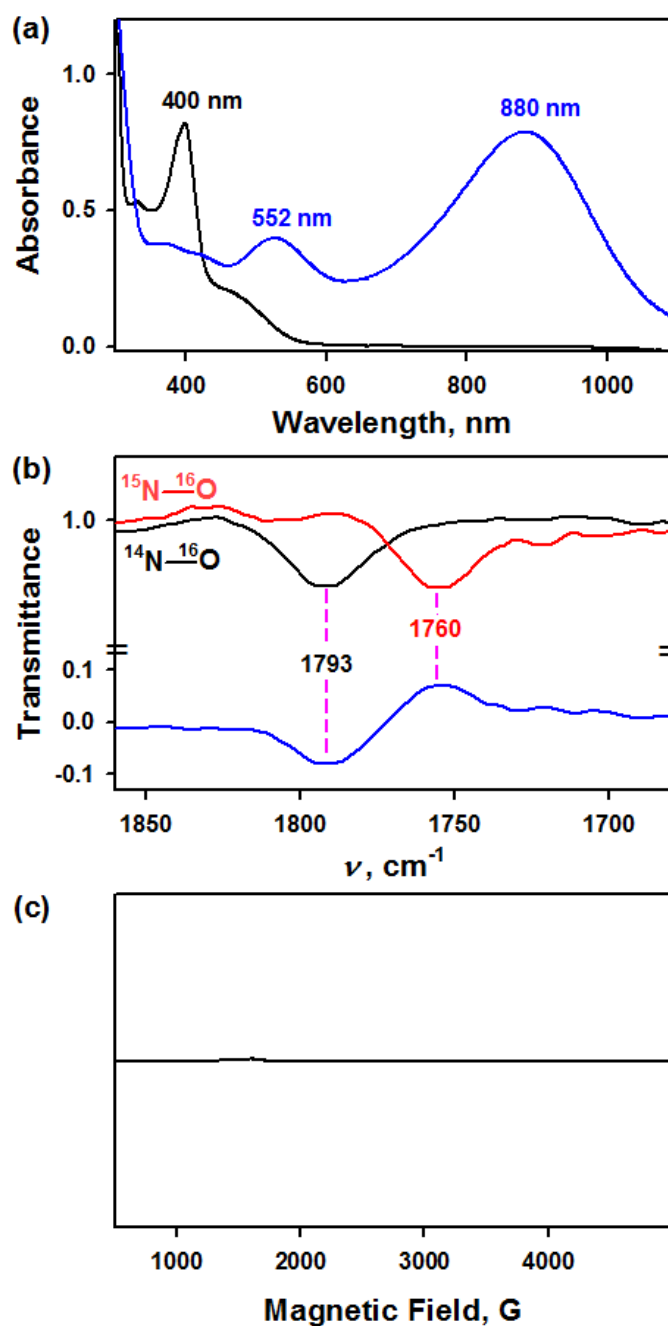
Fig. S2 (a) UV-vis spectra of $[Fe^{III}(TAML)]^-$ (0.10 mM, black line) and $[(TAML)Fe^{IV}(NO)]^-$ (0.10 mM, blue line) under an Ar atmosphere in CH_3CN at -40 °C. (b) Solution IR spectra of **1-^{14}NO** (black line) and **1-^{15}NO** (red line) produced in the reaction of $[Fe^{III}(TAML)]^-$ (5.0 mM) and excess $^{14}NO_{(g)}$ and $^{15}NO_{(g)}$, respectively, under inert atmosphere in CH_3CN at -40 °C. Blue line shows the spectral difference between solution IR spectra of **1-^{14}NO** and **1-^{15}NO**. (c) X-band EPR spectra of **1** (1.0 mM) recorded at 5 K in CH_3CN.
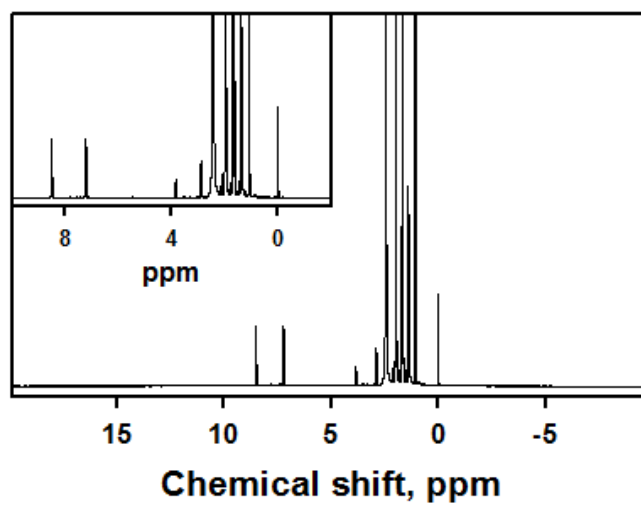
Fig. S3 ^{1}H NMR spectrum of **1** (1.0 mM) in CD$_3$CN at −40 °C.
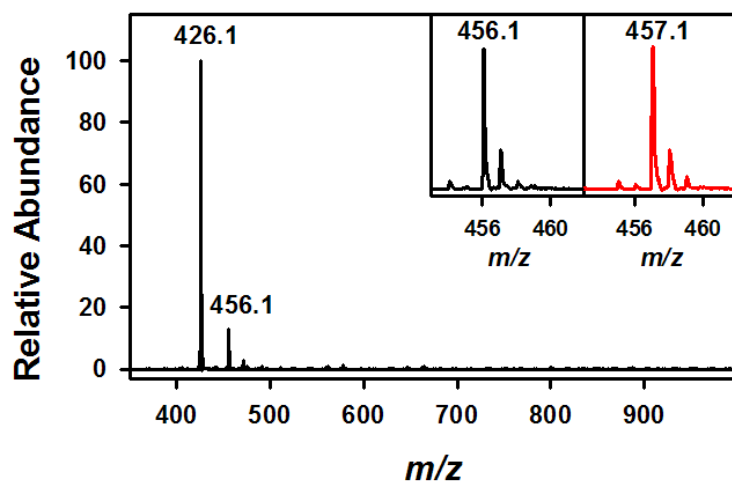
Fig. S4 CSI MS spectra of the reaction solution of **1** in negative mode recorded under inert atmosphere in CH$_3$CN at -40 °C. The peaks at *m/z* of 426.1 and 456.1 are assigned as [Fe(TAML)]$^-$ (calculated *m/z* of 426.1) and [(TAML)Fe(^{14}NO)]$^-$ (calculated *m/z* of 456.1), respectively. Insets show the isotopic distribution patterns of [(TAML)Fe(^{14}NO)]$^-$ (left panel) and ^{15}N-labeled [(TAML)Fe(^{15}NO)]$^-$ (right panel) when the reaction was performed with ^{14}NO$_{(g)}$ and ^{15}NO$_{(g)}$, respectively (see Experimental section for detailed synthetic procedure).
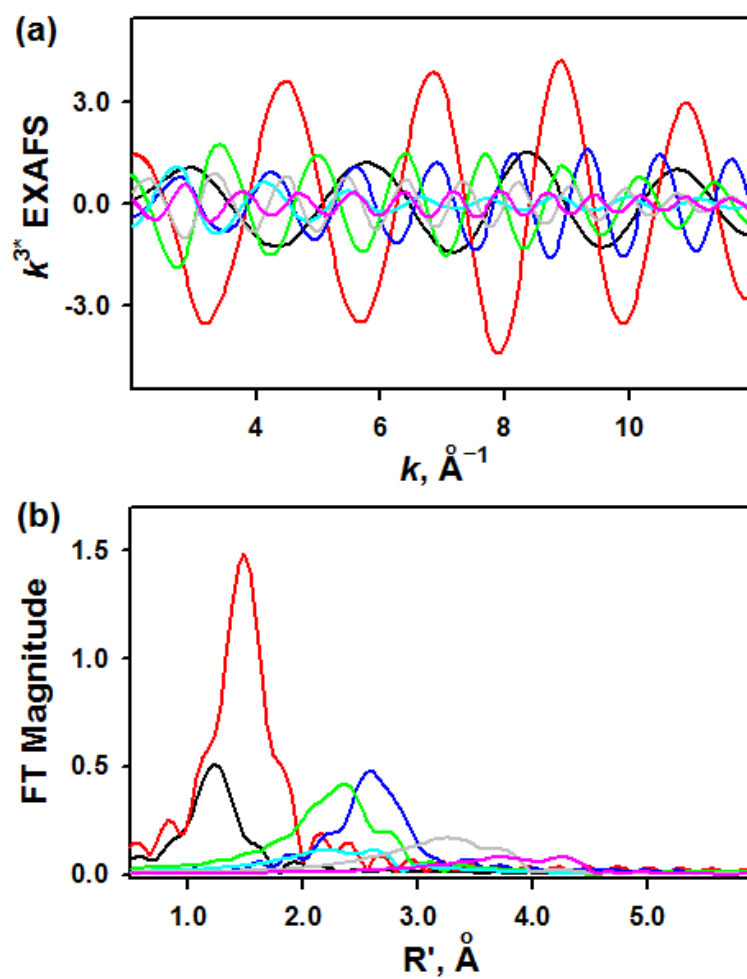
Fig. S5 (a) EXAFS and (b) Fourier Transform of **1** showing fit components 1 (black line), 2 (red line), 3 (blue line), 4 (green line), 5 (cyan line), 6 (gray line), 7 (pink line) (See Table S4).
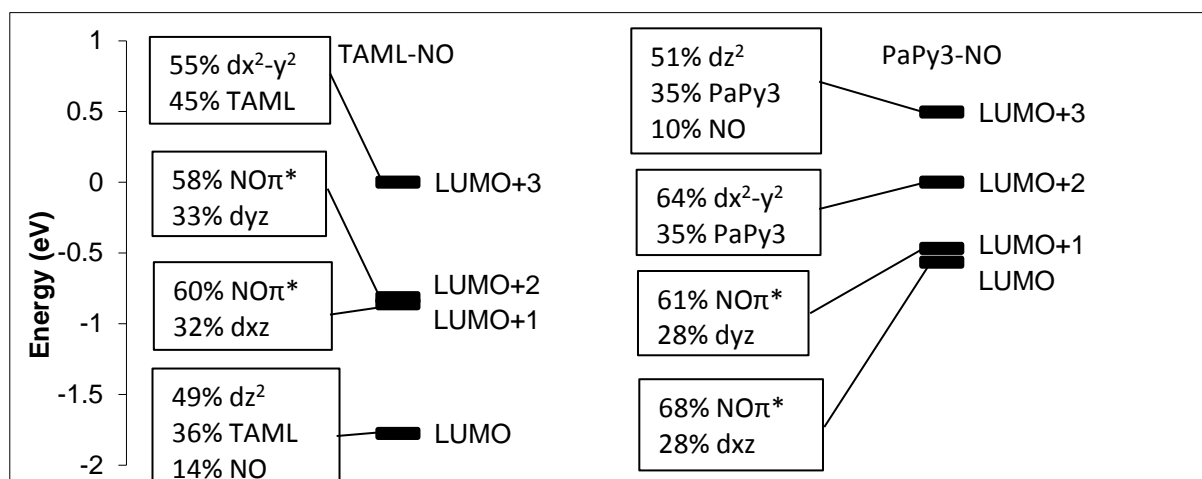
Fig. S6 BP86 calculated molecular orbital energy diagram for **1** and $[(PaPy_3)Fe^{III}(NO)]^{2+}$. The lowest four unoccupied α molecular orbitals for both **1** and $[(PaPy_3)Fe^{III}(NO)]^{2+}$ are shown, along with their Mulliken population analysis. Since the compounds have unpolarized electronic structures, the β orbitals are the same as the α orbitals, and have been omitted for clarity. The primarily dx^2-y^2 orbitals (LUMO+3 for **1**, LUMO+2 for $[(PaPy_3)Fe^{III}(NO)]^{2+}$) are set to 0 eV to show relative orbital energies. As seen from the calculations, in going from the 5-coordinate **1** to the 6-coordinate $[(PaPy_3)Fe^{III}(NO)]^{2+}$, the dz^2 orbital moves up in energy from the LUMO to the LUMO+3.
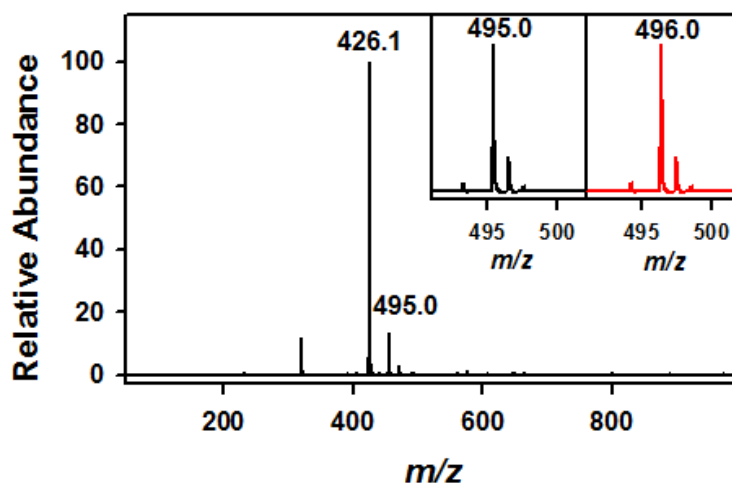
Fig. S7 CSI MS spectrum of isolated **2** in negative mode prepared in the reaction of $[Fe^{III}(TAML)]^-$ (0.10 mM) with $NaNO_2$ (5.0 equiv) under an Ar atmosphere in CH_3CN at $-40\ ^oC$. The peaks at $m/z = 426.1$ and 495.0 are assigned to $[Fe^{III}(TAML)]^-$ (calculated $m/z = 426.1$) and $\{Na[(TAML)Fe(NO_2)]\}^-$ (calculated m/z of 495.1), respectively. Insets show the isotopic distribution patterns of the peaks at m/z of 495.0 for **2-^{14}NO$_2$** (left panel) and m/z of 496.0 for **2-^{15}NO$_2$** (right panel), which were generated by $Na^{14}NO_2$ and $Na^{15}NO_2$, respectively.
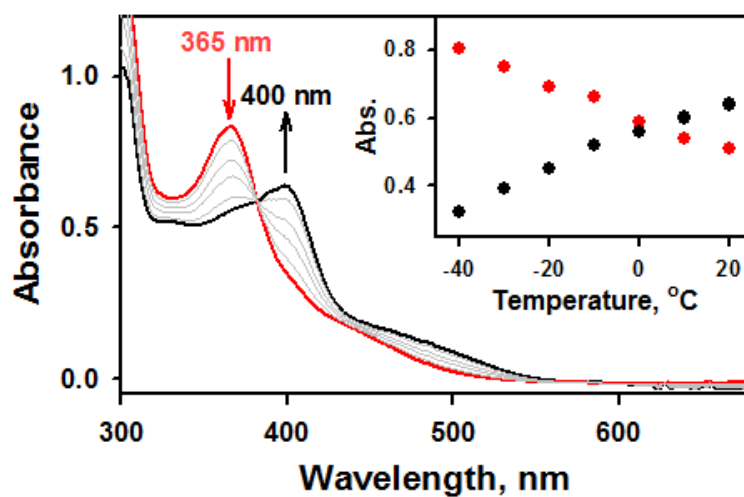
Fig. S8 UV-vis spectral changes of **2** (red line) by increasing temperature from −40 (red line) to 20 °C (black line) in CH$_3$CN. Inset shows the absorbance changes observed at 365 nm (red dot) and 400 nm (black dot).
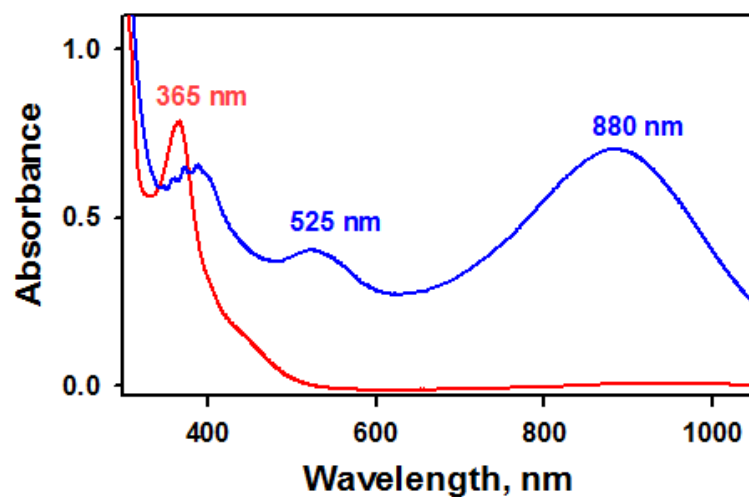
Fig. S9 UV-vis spectra of **2** (red line) and **1** (blue line) produced by the nitrite activation reaction of **2** upon addition of 2.4 equiv of triflic acid (CF$_3$SO$_3$H) to an CH$_3$CN solution containing **2** and 1.2 equiv of ferrocene under an Ar atmosphere at −40 °C.
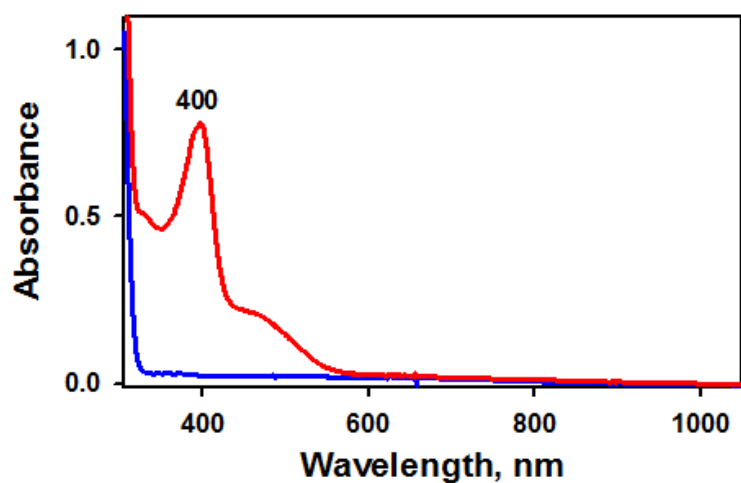
Fig. S10 UV-vis spectra obtained upon addition of [Fe^{III}(TAML)]$^-$ (red line) into a CH$_3$CN solution (blue line) contaning [1.2 equiv of NaNO$_2$, 5.0 equiv of 15-crown ether (15C5), and 1.2 equiv of ferrocene] under an Ar atmosphere at −40 °C.
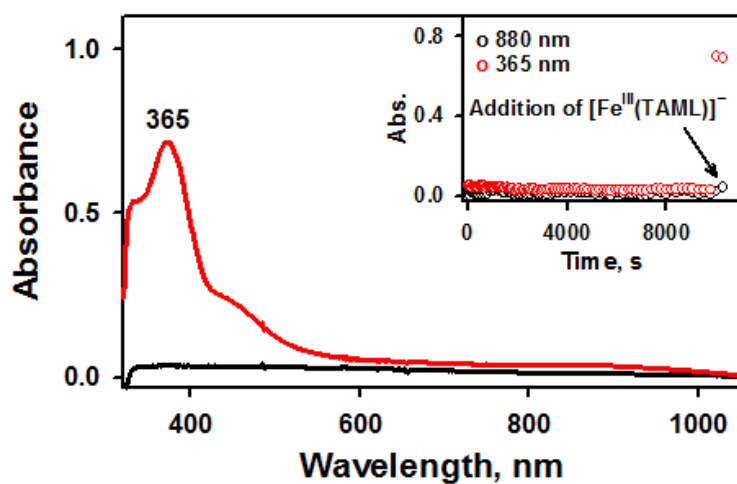
Fig. S11 UV-vis spectra obtained upon addition of $[Fe^{III}(TAML)]^-$ (red line) into a 2.5 h photoirradiated acetone solution (black line) contaning [1.2 equiv of $NaNO_2$, and 5.0 equiv of 15C5] under an Ar atmosphere at $-40\ ^oC$. Inset shows the time course recorded during photolysis of an Ar-saturated acetone solution containing [1.2 equiv of $NaNO_2$, and 5.0 equiv of 15C5] and after addition $[Fe^{III}(TAML)]^-$ complex.
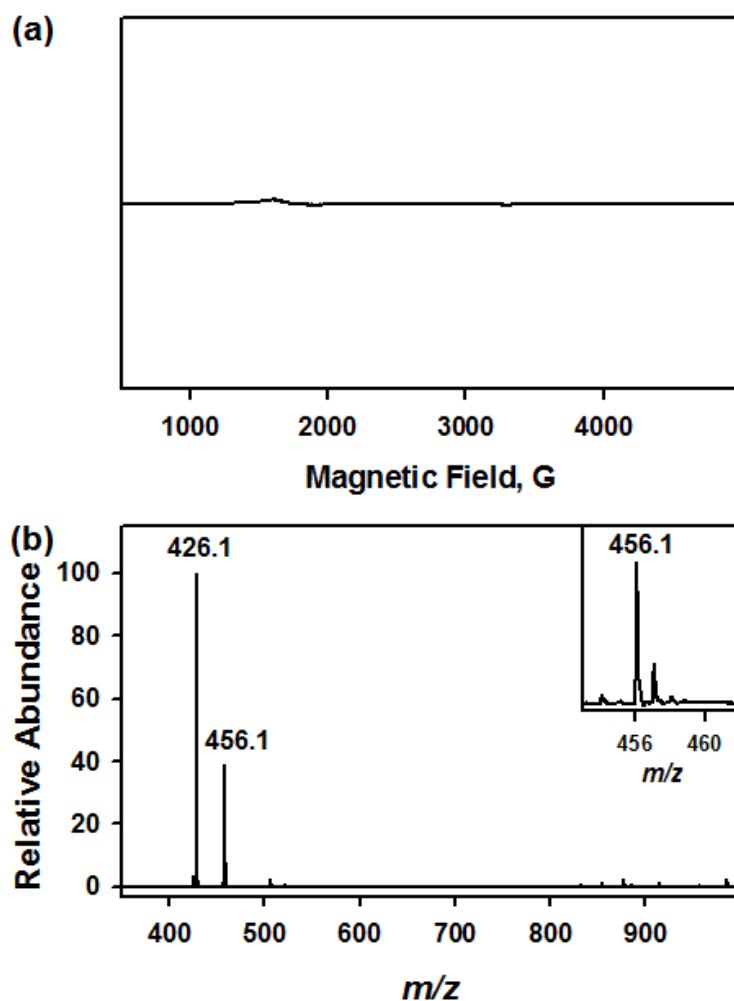
Fig. S12 (a) X-band EPR spectrum of the complete reaction solution obtained in the nitrite activation reaction of **2** (1.0 mM) under photoirradiation in acetone at −40 ℃. Spectrum was recorded at 5 K. (b) CSI MS spectrum of **1** in negative mode obtained in the nitrite activation reaction of **2** (1.0 mM) under photoirradiation in acetone at −40 ℃. The peaks at *m/z* of 426.1 and 456.1 are assigned to [Fe(TAML)]⁻ (calculated *m/z* of 426.1) and [(TAML)Fe(NO)]⁻ (calculated *m/z* of 456.1), respectively. Inset shows the isotopic distribution patterns of the peak at *m/z* of 456.1.